Counterion Effect on the Rheology and Morphology of Tailored Poly(dimethylsiloxane) Ionomers

Ashish Batra and Claude Cohen*

School of Chemical and Biomolecular Engineering, Olin Hall, Cornell University, Ithaca, New York 14853

Hansoo Kim and Karen I. Winey

Materials Science and Engineering Department, University of Pennsylvania, Philadelphia, Pennsylvania 19104

Nozomi Ando and Sol M. Gruner

Department of Physics, Clark Hall, Cornell University, Ithaca, New York 14853

Received October 21, 2005; Revised Manuscript Received December 5, 2005

ABSTRACT: We have carried out a systematic study of the time-dependent rheology and morphology of poly(dimethylsiloxane) (PDMS) ionomers with tailored number of monomers between ions and number of ions per chain as a function of the cation. Small-angle X-ray scattering (SAXS) and scanning transmission electron microscopy (STEM) were used to examine the structure of the samples. The flow behavior of nonequilibrated freshly precipitated ionomers varies from flowing liquids to weak networks. Low mol % zinc and cobalt ionomers that flow do not show aggregates in STEM images whereas gallium, barium, and high mol % zinc ionomers that precipitate as gels show a diverse range of aggregates. The equilibrium state of all ionomers is reached very slowly at room temperature or more rapidly at high temperatures and is a physically cross-linked network irrespective of the cation. Very different morphologies were observed for different cations. Low mol % (∼1 mol %) barium ionomers have rod-shaped and spherical ionic aggregates; gallium ionomers have inhomogeneously distributed highly polydisperse spherical aggregates; and low mol % zinc and cobalt ionomers have no aggregates whereas high mol % (∼7.4 mol %) zinc ionomers have spherical and rodlike aggregates. The nature of the cation has little influence on the elastic modulus of the equilibrated samples.

1. Introduction

The effects of the neutralizing metal cation on the rheology of ionomers have been studied extensively for random ionomers of poly(ethylene-*co*-methacrylic acid) (EMAA) and sulfonated poly(styrene) (SPS) ionomers.[1,2] However, the random arrangement of ions in these ionomers makes it difficult to relate rheology to the structure.[3] Moreover, it is difficult to obtain similar chain length distribution between two copolymers, making it hard to isolate the effect of the cation. Model halatotelechelic polymers (HTPs), which are linear chains or star-shaped polymers with ionic groups at each end, have been examined with some success in relating the rheology to the structure as revealed by small-angle X-ray scattering.[4−8] With the exception of model polyurethane ionomers,[9−14] however, only a limited number of studies have examined rheology−morphology as a function of the cation on model ionomer systems where the number of monomers between ions and the number of ions per chain can be controlled.

Until recently, the morphology of ionomers was inferred primarily from SAXS[15−20] and anomalous SAXS[21−25] patterns. The typical features observed are a broad peak, called the ionomer peak at a momentum transfer vector q in the range of 0.06−0.35 Å^{-1}, as well as a strong upturn in scattered intensity below ∼0.05 Å^{-1}. The position and intensity of these features are dependent on the ion concentration, polymer backbone, and cation used.[22] The upturn is associated with an inhomogeneous distribution of ionic aggregates.[5,21] The broad peak has been interpreted as due to scattering from spherical ionic aggregates with a dimension of 1−10 nm. The scattering mechanisms proposed are either intraparticle interference[15−17] or interparticle[18−20] interference. The model most widely accepted is based on interaggregate interference and was proposed by Yarusso and Cooper.[18] Their model assumes that aggregates are hard spheres distributed with liquidlike order in the polymer matrix. The structural information obtained by fitting the SAXS patterns to the Yarusso−Cooper model is the interaggregate distance, the size of the aggregate, and the total volume of material per ionic aggregate.

In contrast, scanning transmission electron microscopy (STEM) can provide model independent information on ionomer morphology by direct imaging of the shape, size, and distribution of ionic aggregates. A rich diversity of shapes and sizes has been revealed by use of different cations and polymer backbones in the past few years.[26−31]

The ionomers studied here are made from a highly flexible amorphous elastomeric polymer, poly(dimethylsiloxane), PDMS, that has extremely low $T_g = -125$ °C and $T_m = -50$ °C. The flexibility and liquid elastomeric nature of PDMS at room temperature can cause aggregates to form into morphologies that differ from conventional model polyurethane- or polystyrene-based amorphous ionomers. Here we compare the as-precipitated nonequilibrium state[32] and equilibrium state rheology and morphology (via STEM and SAXS) of tailored poly(dimethylsiloxane) ionomers with controlled number of monomers between barium, gallium, zinc, or cobalt cations and the number of cations per chain. The equilibrium state was achieved by heating ionomers to high temperatures for a few days or by aging them at room temperature for months.

10.1021/ma052275a CCC: $33.50
Published on Web 01/26/2006

Table 1. Molar Mass and Polydispersity of OH-Terminated PDMS Precursors Used for the Synthesis of Ionomers

precursor chains	M_n (kg/mol)	M_{peak} (kg/mol)	PDI
1K	0.86	1.1	1.47
7K	6.5	6.7	1.22
9Ka	8.6	8.5	1.32
9Kb	9.3	9.1	1.32

Table 2. Molar Mass and Polydispersity of the Polymers Used in This Study

polymer chains (precursor-fraction-ion)	M_n (kg/mol)	M_{peak} (kg/mol)	PDI	no. of COO^- per chain
Zinc Samples				
1K-f1-Zn				15−18
7K-f2-Zn	38.9	50.3	1.49	6
9Ka-f1-Zn	36.0	53.8	1.63	5
Barium Samples				
7K-f1-Ba		50.2		6
7K-f2-Ba	22.7	31.2	1.37	3
9Kb-f1-Ba		63.8		6
9Kb-f2-Ba		37.0		3
Gallium Samples				
7K-f1-Ga		40.9		5
7K-f2-Ga		20.7		2
9Kb-f1-Ga		55.7		5
9Kb-f2-Ga		25.4		2

2. Experimental Section

2.1. Synthesis of Tailored Polydimethysiloxane with Interacting Groups. The synthesis scheme involves a polycondensation reaction of hydroxyl-terminated PDMS of low polydispersity with a dichlorosilane compound containing a *tert*-butyl protected carboxylic acid group, allowing the incorporation of COO^- at fixed intervals. These intervals are determined by the molar mass of the precursor OH−PDMS−OH. Table 1 shows the molar mass (M_n), the molar mass corresponding to the peak position of the gel permeation chromatograph (M_{peak}), and polydispersity index (PDI) of the OH−PDMS−OH precursors. The precursor names are rounded-off values of M_{peak}. Cleavage of *tert*-butyl group with ppm concentrations of triflic acid catalyst yields the acid form (hereafter called PDMS−COOH samples). To make ionomers, PDMS−COOH solutions are neutralized with 100% excess of barium(II), zinc(II), or gallium(III) acetylacetonate. The final step is a fractionation in a good/bad solvent mixture to yield fractions with moderate polydispersity. The details of the synthesis scheme are reported elsewhere.[32]

Table 2 lists the ionomers used in this study with their M_n, M_{peak}, PDI, and the average number of COO^- groups per chain. The nomenclature used is as follows: 7K-f2-Zn indicates 7K precursor chains, fraction 2, and counterion Zn. 7K-Zn indicates the unfractionated ionomer sample made from 7K precursor chains, counterion Zn, and recovered by evaporation of toluene. For many samples that precipitate as gels, the determination of their M_n and PDI is not straightforward using GPC because the chromatographs are multimodal distributions. For these samples, the lowest molar mass peak is expected to represent the unaggregated ionomer and is used to characterize the ionomers. The average number of COO^- groups is calculated as $\{(M_{peak}/M_n \text{ of precursor PDMS}) - 1\}$ with the assumption that there are no COO^- groups at the ends. However, there will be a fraction of chains that do have COO^- groups at the ends in which case the average number of COO^- groups would be $\{(M_{peak}/M_n \text{ of precursor PDMS}) + 1\}$. For consistency, we assumed there are no COO^- end groups to characterize the ionomers used here.

2.2. Rheology. Dynamic frequency sweeps were carried out with a Rheometrics RDA II rheometer in a parallel plate geometry with 10 mm diameter plates to characterize the storage, loss moduli, and complex viscosities for different temperature conditions.

2.3. Scanning Transmission Electron Microscopy. Thin specimens for scanning transmission electron microscopy (STEM) were prepared using a Reichert-Jung Ultracut S equipped with a diamond knife and a cryo unit operated at −150 °C. Sections of ∼50 nm nominal thickness were collected on standard electron microscopy grids. This solvent-free cryo-method of making sections maintains the bulk property of the ionomers.

Electron microscopy was performed on a JEOL 2010F analytical electron microscope equipped with a Gatan image filter (GIF) and a high angle annular dark field (HAADF) detector for STEM imaging. In the HAADF detection mode, high atomic number elements (e.g., metal cations) appear bright relative to the lower atomic number elements (e.g., carbon). Typical STEM imaging conditions are as follows: 197 kV, 0.7 nm probe size, 150 mm condenser aperture, 512 × 408 pixels, 100 000 to 1 000 000 magnification, and ∼30 s exposure. Final stigmation correction and focusing were performed before moving the specimen to an adjacent and previously unexposed region for image collection. Using this low-dose method, particularly at the higher magnifications, images remain constant during exposure with no detectable beam damage.

The sizes of the various types of ion-rich aggregates were measured (>40 objects measured per morphology), and the mean sizes are reported. In 7K-f1-Ba the electron energy loss spectra were collected in spot mode using the GIF with a 70 μm condenser aperture, a 0.7 nm probe, and a collection time of 2−3 s for core excitations. At these conditions the energy resolution is 1.5 eV. Peak intensities from the core electron energy loss spectra correspond to the cation concentration.

2.4. X-ray Scattering. Cu Kα X-rays (λ = 1.54 Å) were generated using a Rigaku RU-H3R rotating anode X-ray generator equipped with a microfocus cup. The resultant X-ray beam was Ni-filtered and then focused by crossed Franks mirrors. X-ray scattering images were obtained with a custom CCD X-ray detector similar to that described previously.[33] Silver stearate (long spacing = 48.68 Å) and silver behenate (long spacing = 58.38 Å) were used to calibrate the dimension of the scattering vector, $q = 4\pi/\lambda \sin\theta$. Detector-to-sample distances were varied to cover both small-angle and wide-angle X-ray scattering regions. Ionomer samples were prepared for X-ray scattering by pressing between Kapton windows in a 127 μm thick copper ring with an inner diameter of 4 mm. The samples were held on X-ray specimen stage in a thermostated copper jacket.

3. Results and Discussion

3.1. Rheology of Barium Ionomers. Figure 1a shows the rheology of barium ionomer samples 9Kb-f1-Ba and 7K−f1-Ba 1 day after their fractionation and drying at 50 °C to remove excess toluene or methanol. For both materials the storage moduli are greater than the loss moduli, and the complex viscosities show a power law behavior in the frequency range (0.01−100 rad/s). We interpret this to indicate the formation of a weak gel due to the formation of physical cross-links, which could be (1) isolated barium carboxylate triplets consisting of one barium (Ba^{2+}) ion and two carboxylate ions (COO^-) belonging to different polymer chains or (2) ionic triplets aggregated due to electrostatic interactions. Both samples have ∼6 ions per chain. If the number of ions per chain is reduced to a 2−3 ions per chain, samples (9Kb-f2-Ba and 7K-f2-Ba) precipitate as polymers that flow and have a zero-shear viscosity. But, similar to the case of zinc ionomers reported in a previous publication,[32] this is a nonequilibrium state which is manifested by an increase in viscosity over time and the eventual formation of a network. Also, similar to zinc ionomers, the formation of a network is faster at higher temperatures, and the likely reasons for this behavior have been discussed previously.[32]

Figure 1b shows the equilibrium network that forms upon annealing 9Kb-f1-Ba for 264 h at 150 °C. The storage modulus is almost completely independent of frequency over many orders of magnitude indicating the formation of a network with few

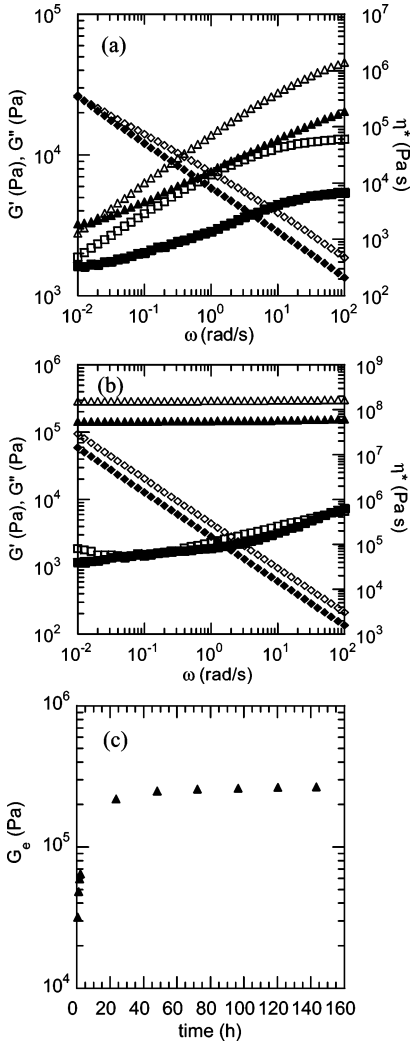

Figure 1. (a) (□) G'', (△) G', (◊) η^* for 9Kb-f1-Ba at 25 °C a day after precipitation and drying; (■) G'' (▲) G', (♦) η^* for 7K-f1-Ba at 25 °C a day after precipitation and drying. (b) (□) G'', (△) G', (◊) η^* for 9Kb-f1-Ba after 264.3 h at 150 °C and (■) G'' (▲) G', (♦) η^* after cooling to 25 °C. (c) Evolution of the equilibrium modulus (G_e) for 9Kb-f1-Ba at 150 °C.

structural defects that dissipate energy in this range of frequency. The formation of a network with few defects is similar to what we reported for zinc and sodium PDMS ionomers.[32] The value of the storage modulus decreases on cooling from 150 to 25 °C in a similar fashion as for end-linked PDMS networks. The evolution of the elastic modulus at 150 °C for 9Kb-f1-Ba is shown in Figure 1c. The elastic modulus was approximated as the value of the storage modulus at 0.1 rad/s. A value of molar mass between effective cross-links M_c can be calculated from the elastic modulus using $M_c = \rho RT/G_e$, where G_e is the elastic modulus, ρ is the density of the polymer, and T is the temperature. From the measured value of G_e at 264.3 h, for 9Kb-f1-Ba a M_c value of 12K is calculated. Thus, at least 75% (9K/12K) of ions form ionic triplets and consecutive ions along a chain form elastic strands. This number is similar to the number for zinc and sodium ionomers, reaffirming the conclusion drawn previously that once the equilibrium structure is reached, the nature of the cation has little influence on the equilibrium modulus achieved. The latter is governed by the length of the elastic chain between ions. A possible reason for this result is presented later when discussing STEM images of the equilibrium structures of ionomers with similar ion concentration and number of ions per chain but different cation.

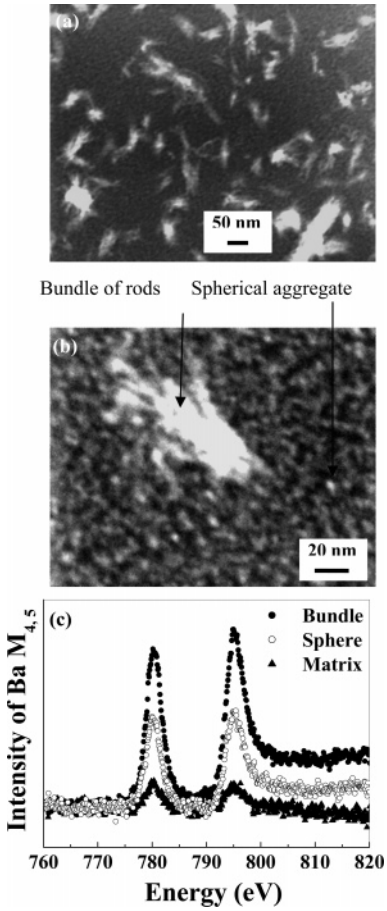

Figure 2. HAADF-STEM images of 7K-f1-Ba stored 3 months after precipitation. (a) Image shows Ba-rich bundles of rods. (b) Image shows detail of a Ba-rich bundle of rods and smaller spherical Ba-rich domain. (c) EELS intensity of Ba $M_{4,5}$ peaks collected from the bundles, the spherical domains, and the matrix, indicating that Ba is detected in all three regions while showing differences in concentration of the cation.

3.2. STEM of Barium Ionomers. Figure 2a shows the HAADF-STEM image of the 7K-f1-Ba 3 months after precipitation and drying. Two shapes of barium ionic aggregates can be distinguished in Figure 2b. One is a bundle of rodlike structures, and the other is smaller spherical aggregates. There is considerable overlap of the spherical aggregates due to image projection in the STEM, indicating that the aggregates are in close proximity in the Ba-neutralized material. These Ba-rich aggregates appear as bright regions in these HAADF-STEM images because they have a higher average atomic number than the matrix. Figure 2c shows core loss EELS spectra in the energy region corresponding to the two expected Ba $M_{4,5}$ transitions. The intensities of these Ba peaks correspond to the relative concentrations of Ba in the bundle, sphere, and matrix. These spectra confirm the interpretation of the STEM images referring to the bundles and spheres as Ba-rich ionic aggregates. The spectrum for the matrix suggests the presence of Ba in the matrix, though this is difficult to quantify. The probe size is comparable to the distance between the spherical ionic aggregates so that the slightest drift might detect Ba contained in the aggregates while nominally probing the matrix. With these results we demonstrate that with further refinement, EELS may be a potentially useful technique to study the local chemical composition of ionomers. The diameter of the spherical aggregates is ∼4 nm; the diameter of individual rods in the bundles of rods is ∼4 nm, and the typical length of the rods is ∼60 nm. Such high aspect ratio (>10) ionic aggregates have never been reported in ionomers.

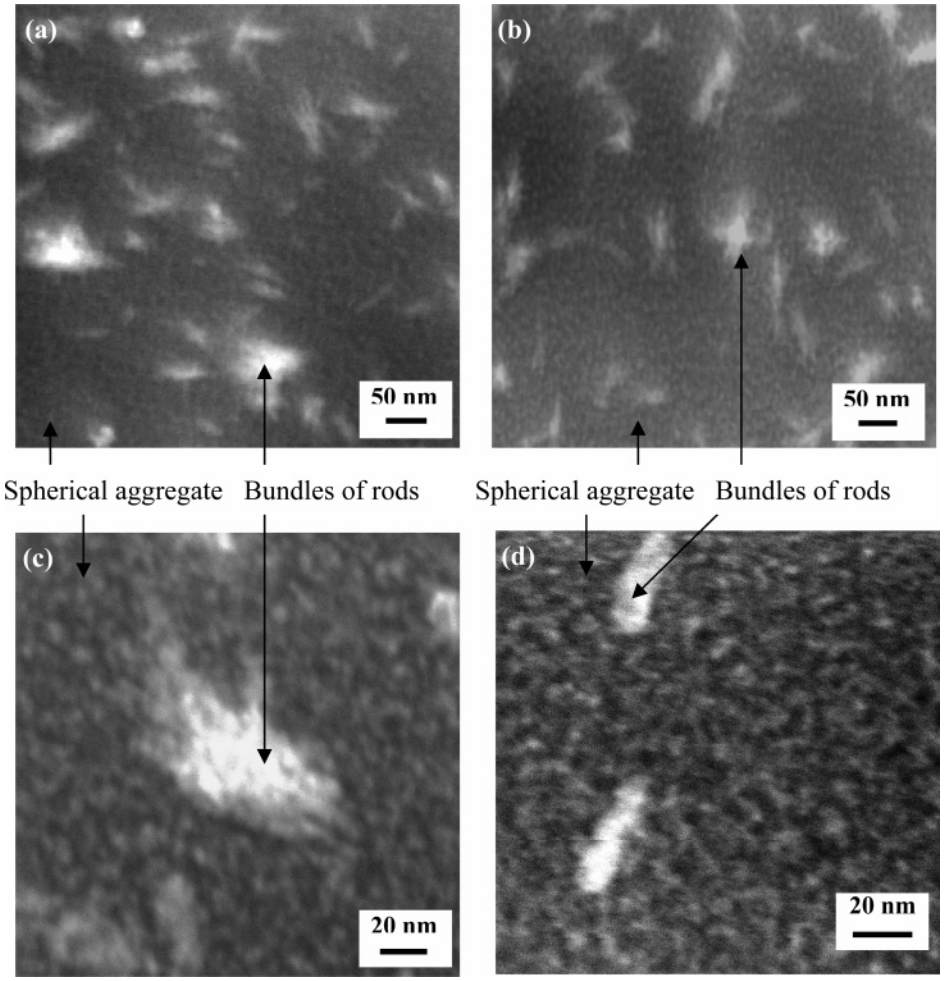

Figure 3. HAADF-STEM images of 7K-f1-Ba following precipitation, drying, and the following annealing conditions: (a) annealed at 150 °C for 5 days, (b) annealed at 150 °C for 20 days, and (c) held at room temperature for 5 months. (d) HAADF-STEM images of 7K-Ba recovered by evaporation of toluene.

Using density and formula weight of a typical barium inorganic salt such as barium acetate, the average volume per atom can be calculated to be 0.0114 nm^3. A barium carboxylate triplet is constituted by 7 atoms, and hence the volume of the barium triplet can be approximated to be 0.08 nm^3 with a diameter of 0.52 nm. The spherical aggregates of diameter 4 nm occupy a volume of 34 nm^3. This would imply that the aggregation number is ∼425 cations per aggregate if only barium carboxylate triplets reside inside the spherical aggregate. It is sterically impossible to have 425 cations connected to polymer chains residing in a single aggregate of the observed size. Thus, the aggregate though barium rich must contain segments of the polymer backbone. A similar argument can be made for the bundles.

Figure 3a shows a STEM image of 7K-f1-Ba after annealing at 150 °C for 5 days whereas Figure 3b shows a STEM image after 20 days of annealing. These images and Figure 3c that shows the sample 5 months after precipitation and drying indicate that the shapes and sizes of aggregates in barium ionomers do not change with time or by annealing at 150 °C. Assuming that the mobility of polymer chains that are part of these large bundles of rods is significantly reduced, it is possible that the rod-shaped structures in the bundles may represent a trapped nonequilibrium shape. Similar arguments have been made by Taubert et al.[31] to explain formation of chainlike assemblies of spheres in polyimide ionomers.

Parts a and b of Figure 3 are STEM images of 7K-f1-Ba that has been rheologically characterized as a physical network with an elastic modulus measured at 0.1 rad/s of the order of 0.1 MPa. Figures 2a,b and 3c are STEM images of 7K-f1-Ba from a much weaker physical network with an elastic modulus of the order of 0.02 MPa or lower. The similarity in STEM images but the significant difference in moduli indicates that the increase in modulus on heating does not occur by rearrangement or increase in size of the barium aggregates visible via STEM. As with zinc ionomers, [32] polymer chains reorganize their intramolecular triplets into intermolecular triplets as the network structure of barium ionomers equilibrate, leading to cross-links and stronger networks.

Figure 3d shows a HAADF-STEM image of a 7K-Ba sample that has been annealed to 150 °C for 5 days. This 7K-Ba sample was recovered by evaporation of toluene from the ionomer solution rather than by fractionation from a good/bad solvent mixture, as in the case of 7K-f1-Ba. The number of bundlelike structures is suppressed but the spherical aggregates are present. This indicates that the method of preparation has a marked influence on the morphology on these samples assuming that the difference in polydispersities does not play a role.

Figure 4a shows the HAADF-STEM image of 9Kb-f1-Ba after annealing at 150 °C for 5 days. The basic aggregate shapes are similar to the 7K-f1-Ba. Spheres (∼4 nm in diameter) and rods (∼4 nm in diameter and ∼100 nm in length) are seen in these images. However, the rods are longer for 9Kb-f1-Ba, and hardly any bundles of these rods are observed. We have noted previously for zinc ionomers, that a longer chain length between ions promotes intermolecular interactions.[32] For the barium

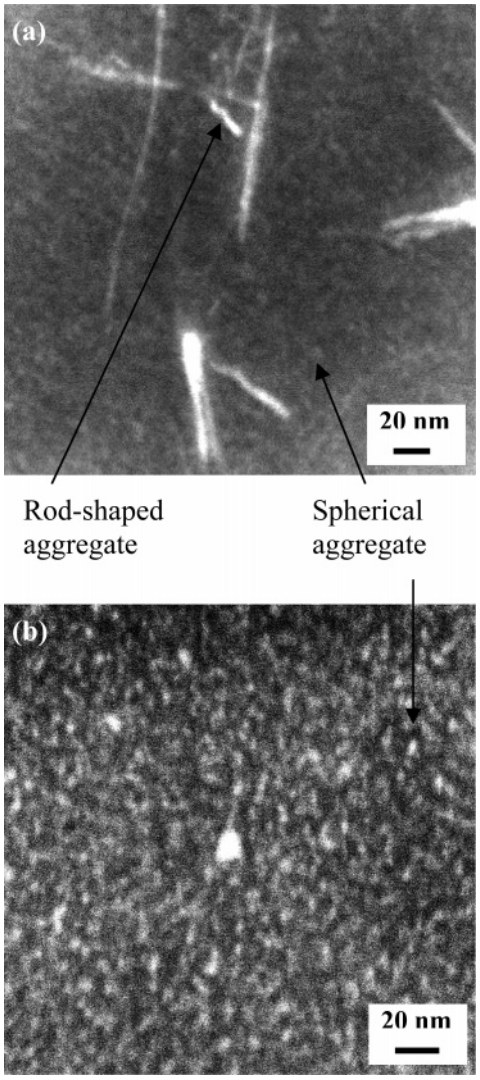

Figure 4. (a) HAADF-STEM image of 9Kb-f1-Ba after annealing at 150 °C for 5 days. (b) HAADF-STEM image of 9Kb-Ba recovered by evaporation from toluene.

ionomers considered here we can then speculate that there would be more intermolecular interactions in 9Kb-f1-Ba than in 7K-f1-Ba (both have a similar number of ions per chain). Thus, an aggregate that pulls ions from many chains would be more extended than one in which many ions come from the same polymer chain.

Figure 4b shows the HAADF-STEM images of 9Kb-Ba recovered by evaporation and annealed to 150 °C for 5 days. Similar to all other barium ionomers, spherical aggregates ~4 nm in diameter are observed. The formation of rods is greatly suppressed, suggesting again that preparation conditions influence morphology of ionomers.

3.3. X-ray of Barium Ionomers. Figure 5a shows the X-ray scattering profiles of the Ba ionomers in the q range from 0.01 to 1 Å^{-1} for barium ionomers and a reference PDMS sample. These plots are constructed by combining SAXS and WAXS data and matching the scattering intensity in the common q range. The high q region shows two peaks for the unmodified PDMS sample. The peak at 0.85 Å^{-1} is related to spatial correlations between chain segments of PDMS.[33] The peak at ~0.4 Å^{-1} is due to the Kapton windows. Thus, these peaks must also appear in high q scattering intensity plots of ionomer samples. Scattering intensities in the entire q range of 0.01−1 Å^{-1} are presented for ionomer samples 9Kb-f1-Ba at room

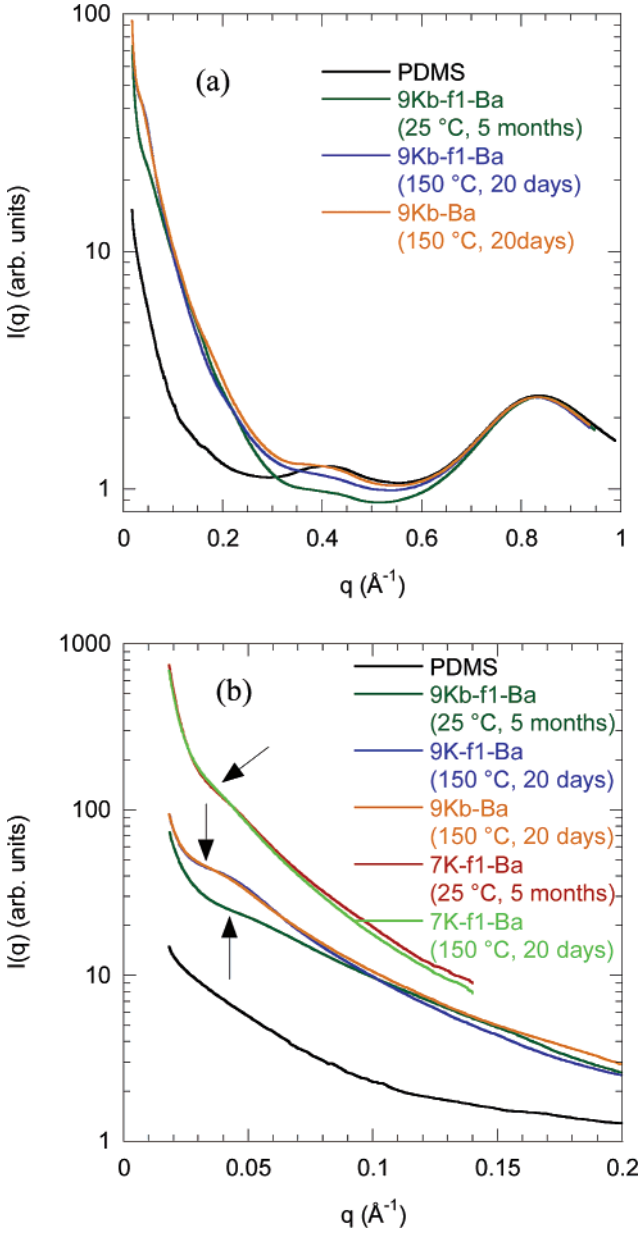

Figure 5. (a) Intensity vs q for PDMS reference, 9Kb-f1-Ba at room temperature 5 months after drying and precipitation, 9Kb-f1-Ba after annealing at 150 °C for 20 days, and 9Kb-Ba recovered by evaporation of toluene and annealing at 150 °C for 5 days. (b) Small-angle region of $I(q)$ vs q plot for 7K-f1-Ba at room temperature 5 months after precipitation and drying, 7K-f1-Ba after annealing at 150 °C for 20 days, and samples shown in (a). Arrows point to the shoulders on the upturn at low q for the respective barium ionomers.

temperature 5 months after precipitation and drying, sample 9Kb-f1-Ba annealed at 150 °C for 20 days, and sample 9Kb-Ba recovered by evaporation and annealed at 150 °C for 20 days. For ease of comparison of the scattering pattern at low q shown in Figure 5b, the peak intensities at 0.85 Å^{-1} for these samples are scaled to the same peak intensity at 0.85 Å^{-1} for the unmodified PDMS. For sample 7K-f1-Ba 5 months after precipitation and drying and sample 7K-f1-Ba annealed at 150 °C for 20 days, only the small angle region was probed, and the intensities are plotted on an arbitrary scale (Figure 5b).

The data from 9Kb-f1-Ba annealed at 150 °C for 20 days and from 9Kb-Ba recovered by evaporation and annealed at 150 °C for 20 days have the same scattering intensity shape and show shoulders on the upturn in the vicinity of 0.03−0.05 Å^{-1}. Such a shoulder on the upturn has been interpreted to be

an ionic peak (due to interaggregate interference) merged with an intensity upturn at low q by Visser and Cooper[34] for sodium neutralized polyurethane ionomers. In the absence of a better defined peak, we will not attempt to fit any model to these X-ray scattering data. However, assuming interparticle interference, the average distance between ionic aggregates can be estimated as $2\pi/q^*$, where q^* is the approximate position of the shoulder in the scattering intensity plots. For 9Kb-Ba recovered by evaporation and 9Kb-f1-Ba annealed at 150 °C for 20 days, $q^* \sim 0.035$ Å^{-1}. This corresponds to an interaggregate distance of ~18 nm, which is much larger than the length scale of the elastic strand of the network as obtained from rheology.

STEM images of these samples show that rod formation is greatly suppressed in the sample recovered by evaporation. Despite this difference in STEM images, the similarity in X-ray scattering data could imply that it is largely the spheres common to both STEM images that result in the scattering peak merged with the upturn. The ~18 nm interaggregate distance would correspond then to the spacing between the spheres in these images. The number of spherical aggregates present in a typical 80×80 nm^2 area was counted (~40−50) in the STEM image of the annealed 9K-f1-Ba annealed for 5 days (Figure 4a). Assuming a nominal thickness of 50 nm for the sample, the number of aggregates per unit volume and hence the volume per aggregate are calculated. The mean interaggregate distance is estimated as the cube root of the volume per aggregate. An approximate mean separation between spheres is found to be ~19 nm, remarkably close to the 18 nm separation estimated from X-ray scattering. STEM could not be carried out with the unannealed sample 9Kb-f1-Ba because it was too soft but the scattering pattern is slightly different from that of the annealed samples. The unannealed 9Kb-f1-Ba 5 months after precipitation and drying shows a shoulder at $q^* \sim 0.045$ Å^{-1} that is not as pronounced as for the annealed samples. This corresponds to an interaggregate distance of ~14 nm.

The shoulders in the scattering upturns for 7K-f1-Ba at room temperature 5 months after precipitation and drying and for 7K-f1-Ba annealed to 150 °C for 20 days occur at ~0.03 Å^{-1}. This corresponds to an interaggregate distance of ~21 nm. From the STEM image of the annealed 7K-f1-Ba annealed for 20 days (Figure 3b), using the same procedure as outlined above an approximate mean separation between spheres is found to be ~18 nm, quite close to 21 nm estimated from X-ray scattering. The interaggregate distance remains constant upon annealing in contrast to the 9Kb-f1-Ba where a slight increase in interaggregate distance was observed. The interaggregate distance for 7K-f1-Ba is greater than 9Kb-f1-Ba. Thus, similar to our observation with STEM images, a slight variation in number of monomers between ions can cause changes in structure and morphology of tailored ionomers.

3.4. Rheology of Gallium Ionomers. Figure 6a shows the rheology of gallium ionomer samples 9Kb-f1-Ga and 7K-f1-Ga 1 day after their fractionation and drying at 50 °C. For both these samples the storage moduli are greater than the loss moduli, and the complex viscosities show a power law behavior in the frequency range (0.01−100 rad/s), indicating the formation of a weak network. In contrast to freshly precipitated barium ionomers, freshly precipitated gallium ionomers have a higher elastic modulus tending toward a plateau at low frequencies. On heating, a gallium ionomer forms a network with few structural defects that dissipate energy in the range of frequencies examined, similar to all ionomers considered in our studies on poly(dimethylsiloxane)-based ionomers. Figure 6b shows the network formation for 7K-f1-Ga after 23 h at 150 °C and after cooling to 25 °C. Cooling again reduces the modulus to a similar extent as observed in end-linked PDMS. Similar to barium ionomers, gallium ionomers (7K-f2-Ga and 9Kb-f2-Ga) with few ions per chain precipitate as polymer that flow but eventually form networks with aging or curing at high temperature.

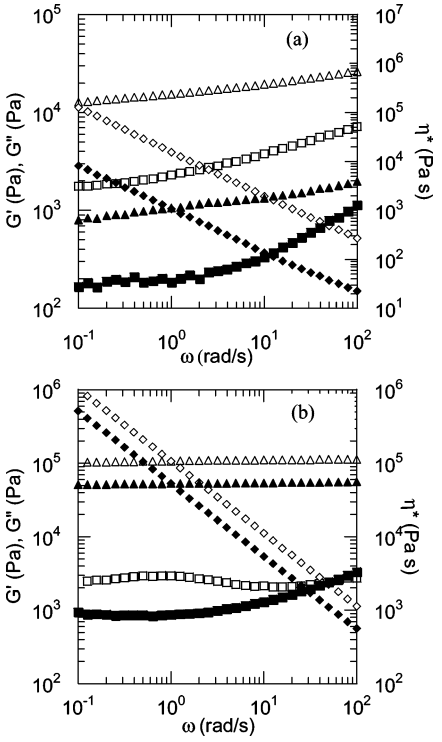

Figure 6. (a) (□) G'', (△) G', (◇) η^* for 9Kb-f1-Ga at 25 °C a day after precipitation and drying; (■) G'' (▲) G', (♦) η^* for 7K-f1-Ga at 25 °C a day after precipitation and drying. (b) (□) G'', (△) G', (◇) η^* for 7K-f1-Ga after 23 h at 150 °C and (■) G'' (▲) G', (♦) η^* after cooling to 25 °C.

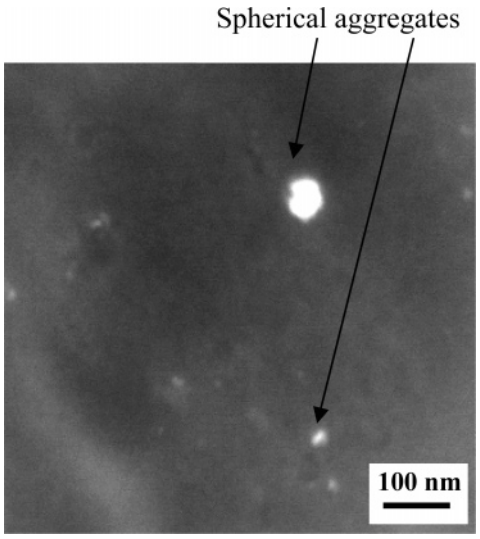

Figure 7. HAADF-STEM image of 9Kb-f1-Ga annealed at 150 °C for 5 days, where bright regions correspond to Ga-rich domains as confirmed by EDS analysis.

3.5. STEM and SAXS of Gallium Ionomers. Figure 7 shows a HAADF-STEM image of 9Kb-f1-Ga annealed at 150 °C for 5 days having an inhomogeneous distribution of spherical aggregates that are polydisperse in size with diameter ~10−60 nm. Energy-dispersive X-ray spectroscopy (EDS) analysis

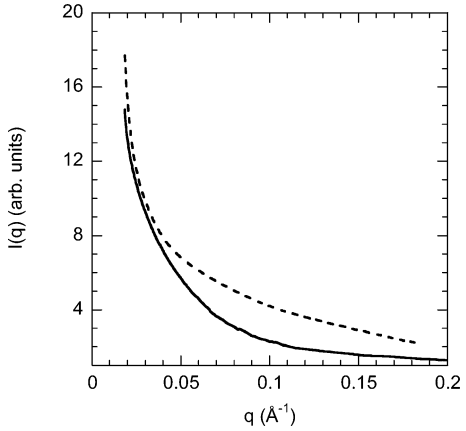

Figure 8. X-ray scattering intensity vs q plot for (—) PDMS reference and (- - -) 9Kb-f1-Ga annealed at 150 °C for 5 days.

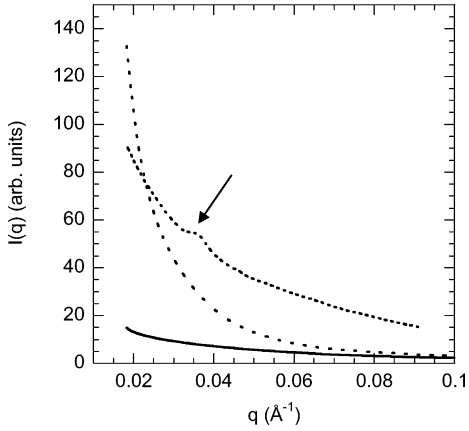

Figure 9. X-ray scattering intensity vs q plot for (—) PDMS reference, (- - -) 7K-f2-Zn annealed at 150 °C for 20 days, and (• • •)7K-Zn recovered by evaporation of toluene and annealed at 150 °C for 20 days.

confirmed that the bright regions correspond to Ga-rich domains. Figure 8 shows the SAXS intensity plot of 9Kb-f1-Ga annealed at 150 °C for 5 days along with a PDMS reference sample. The intensity of the gallium ionomer is shifted vertically in the plot so that the curve remains just above the reference PDMS sample without crossing it. Only an upturn in intensity related to the inhomogeneous distribution of ions is observed. The relatively featureless scattering profile can be related to the sparsely populated STEM image and the subsequent absence of interparticle scattering.

3.6. STEM and SAXS of Zinc and Cobalt Ionomers. Zinc and cobalt ionomers with similar ion concentration and number of ions per chain as 7K-f1-Ba and 7K-f1-Ga were shown in a previous article to precipitate as flowing melts. This is in stark contrast to 7K-f1-Ba and 7K-f1-Ga samples that precipitate as weak networks. This could be attributed to the more ionic character of barium and gallium ionomers than that of the transition metal ionomers of cobalt and zinc. This more ionic character may also be manifested in the aggregate formation observed immediately after precipitation and drying at room temperature of the barium and gallium ionomers. The STEM images (not shown) of 9Ka-f1-Zn annealed to 150 °C for 15 h are featureless, thereby indicating the absence of Zn-rich domains within the detection limit (∼0.5 nm) of this method. On the basis of these data and similar images for cobalt, we have concluded that aggregates do not form in low ion concentration transition metal PDMS ionomers.[32] Thus, it is reasonable to argue that aggregate formation leads to the lack of fluidity ($G' > G''$) of ionomers in the freshly precipitated state.

In our previous article[32] we reported a difference in the FTIR spectrum of low mol % zinc samples precipitated vs those recovered by direct evaporation of the solvent and speculated that different morphologies may exist in these samples. Figure 9 shows the SAXS patterns of 7K-f2-Zn prepared by neutralization with a stoichiometric quantity of zinc acetylacetonate and a 7K-Zn evaporated sample, both annealed at 150 °C for 20 days. All intensities are plotted on an arbitrary scale. No ionic peaks or shoulders on upturns are observed for the fractionated sample, which correlates with the lack of features in the STEM image. The evaporated sample shows a SAXS pattern that is different from the fractionated sample in the shape of the upturn, and a weak peak at $q^* \sim 0.035$ Å^{-1} corresponding to an interaggregate distance of ∼18 nm is observed. Although, STEM for the evaporated sample could not be carried out due to sample brittleness, on the basis of SAXS data, we conclude aggregates are present. Assuming we can ignore the differences in the molar mass polydispersities of the samples, this shows again that preparation conditions can influence the morphology of these ionomers.

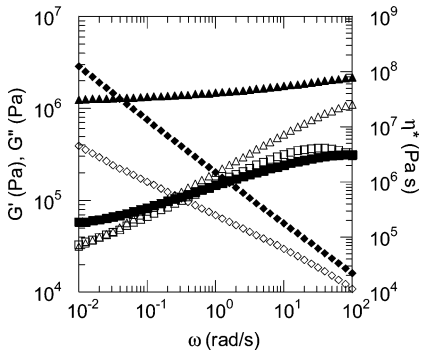

Figure 10. (△) G', (□) G'', (◇) η^* for 1K-f1-Zn 1 day after precipitation and drying; (▲) G', (■) G'', (♦) η^* for 1K-f1-Zn after annealing to 150 °C for 5 days.

3.7. High Ion Concentration (7.4 mol %) Zinc Ionomers. Figure 10 shows the rheology of the 1K-f1-Zn sample 1 day after precipitation and drying and after annealing at 150 °C for 5 days. The storage modulus 1 day after precipitation and drying is greater than the loss modulus and the complex viscosity shows a power law in the frequency range considered, indicating the formation of a network due to ionic cross-links. The rheology of this zinc sample proves that when the carboxyl ion concentration is increased dramatically (7.4 mol %) as compared to the low concentrations (0.3−1.3 mol %) studied earlier, even transition metal ionomers of PDMS will precipitate as physical networks as opposed to fluid melts.

The value of the storage modulus is greater than the value of the storage modulus of barium and gallium ionomers discussed above. This is expected given the larger number of ions per chain (15−18) and the smaller number of monomers between ions. A network with a plateau modulus of 1.2 MPa forms on annealing the sample at 150 °C for 5 days. A value of the molar mass between effective cross-links M_c is calculated to be 2.8 kg/mol. Further annealing may result in a stronger network and a smaller molar mass between effective cross-links (closer to the precursor $M_n \sim 1$ kg/mol), but the short distance between ions along the chain may lead to loops that are elastically ineffective and reduce the modulus from what would be expected if most ions are involved in the formation of elastic strands.

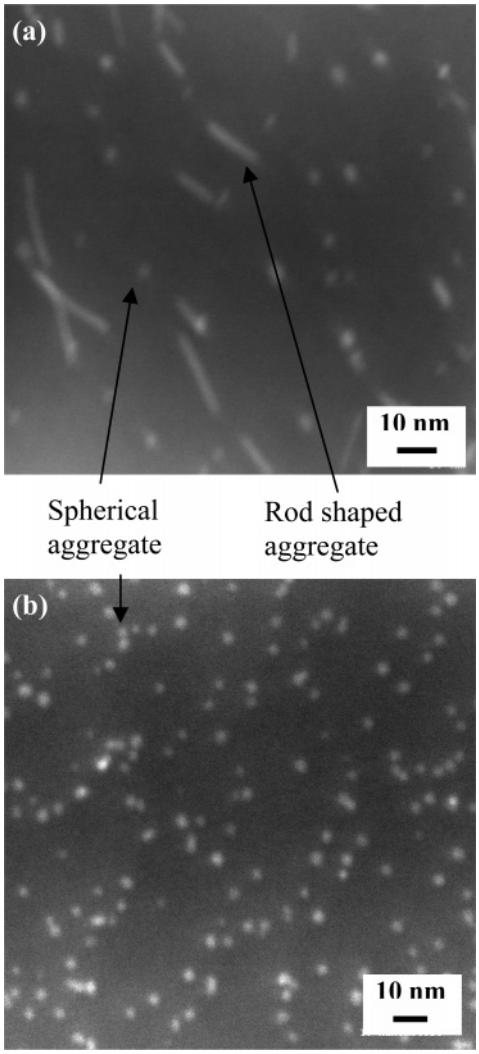

Figure 11. HAADF-STEM images of 1K-f1-Zn following precipitation, drying, and the following annealing conditions: (a) held at room temperature for 3 months; (b) annealed at 150 °C for 5 days.

Figure 11a shows a HAADF-STEM image of 1K-f1-Zn 3 months after precipitation and drying. Two shapes of zinc-rich ionic aggregates can be distinguished in Figure 11a. One is rods with a smaller aspect ratio (∼3) than the rods observed in barium ionomers and the other is spheres. Rods have a diameter of ∼3.6 nm and length of ∼11 nm The spheres have a diameter of 3.6 ± 1.8 nm. Annealing the samples at 150 °C for 5 days converts the rods into spheres. This is shown in Figure 11b, in which only spherical-shaped aggregates can be distinguished. The diameter of spheres is 4.5 ± 0.8 nm.

It can be postulated that, unlike the large barium aggregate for which we speculated that the polymer mobility is drastically reduced, here the smaller rods may not hinder polymer mobility to a great extent and as the ionomers equilibrate the rods break up to form spheres.

If only zinc carboxylate triplets are assumed to reside in a single spherical aggregate ∼4 nm in diameter, calculations similar to those carried out for spherical barium aggregates indicate the presence of 435 zinc cations in a single aggregate of the observed size. Mean interaggregate distance in Figure 11b assuming a thickness of 50 ± 20 nm is calculated to be 17 ± 2 nm. The number of aggregates per unit volume is estimated to be (2 ± 0.9) × 10^{-4} nm^{-3}. In Figure 11b, the number of spherical aggregates has been counted, and assuming a thinkness of 50 nm, we estimate that a maximum of 7.4 × 10^4 zinc cations can be present in aggregates. But knowing the density of the polymer (0.97 g/cm^3) and the ion concentration, we estimate the number of zinc atoms in the same volume to be 10^6 zinc cations. Thus, only 7−8% of zinc cations are present in STEM-detected aggregates and 93% of zinc cations are present as isolated ionic triplets or combinations of two or three triplets not visible via STEM. It is this 93% that governs the equilibrium rheology.

For comparison of the scattering pattern at low q, the peak intensity at 0.85 $Å^{-1}$ for the 1K-f1-Zn ionomer 5 months after precipitation and drying is scaled to the peak intensity of the reference unmodified PDMS (Figure 12a). Despite the aggregates being clearly visible via STEM, the small-angle region of the $I(q)$ vs q plot (Figure 12b) does not show a peak or a shoulder on the scattering upturn at low q. This implies that no significant spatial correlations exist between these aggregates. This is consistent with the observation that only 7−8% of the zinc ions participate in the aggregates. The only relevant feature in the SAXS pattern is the upturn that corresponds to an inhomogeneous distribution of ions in the sample.

All samples that show some aggregates in STEM images (9Kb-f1-Ba, 9Kb-f1-Ga, and 1K−f1-Zn) show deviations from the X-ray scattering pattern of unmodified PDMS that begin at similar q values. However, samples such as 7K-f2-Zn that have a featureless STEM image show deviations from unmodified PDMS at a much lower value of q.

4. Conclusions

We have carried out a systematic structure-flow property relationship study of model poly(dimethylsiloxane) ionomers with controlled number of monomers between ions and number of ions per chain. Diverse rheological behavior is seen with low carboxyl ion concentration (0.7−1.3 mol %) ionomers in the freshly precipitated state. Barium and gallium ionomers freshly precipitated from a good/bad solvent mixture precipitate as weak networks at room temperature, whereas zinc and cobalt ionomers precipitated as flowing melts. Fluidity has been correlated to the lack of aggregates in the nonequilibrium freshly precipitated state. Preparation conditions have also been found to affect the morphology in these ionomers. Table 3 summarizes the results as a function of the cation. The equilibrium state of all ionomers irrespective of the cation is a physically cross-linked network with few structural defects that dissipate energy in the mechanical frequency range examined, but very different

Table 3. Summary of Rheological Properties and Structures of Freshly Precipitated Ionomers as Function of the Cation

	zinc, cobalt (∼1 mol %)	barium (∼1 mol %)	gallium (∼1 mol %)	zinc (7.5 mol %)
moduli	$G'' > G'$	$G' > G''$ no plateau modulus	$G' > G''$ plateau modulus	$G' > G''$ no plateau modulus
viscosity	zero-shear viscosity	power law viscosity	power law viscosity	power law viscosity
SAXS	upturn at very low q	shoulder on upturn at low q	upturn	upturn
STEM	no aggregates	spheres and bundles of rods that do not change shape with time or temperature	inhomogeneously distributed spheres in the annealed state	rods that convert to spheres with heat or time

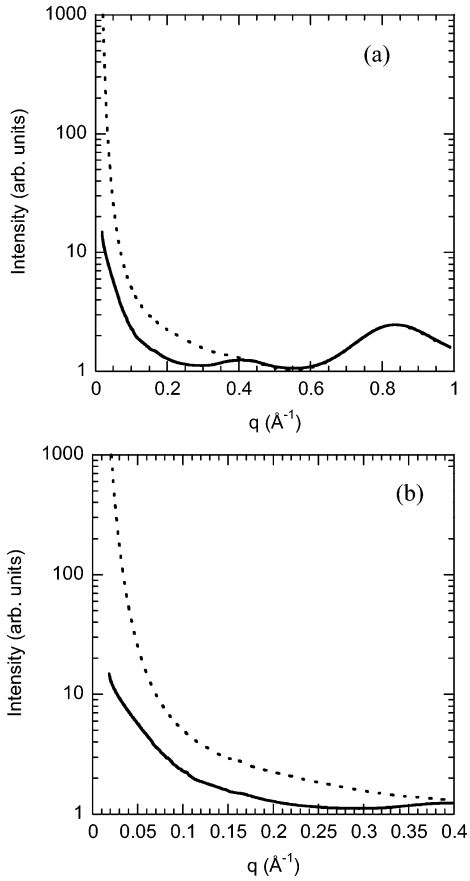

Figure 12. X-ray scattering intensity vs q plot for (—) PDMS reference, (- - -) 1K-f1-Zn 5 months after precipitation and drying. (b) Small-angle region of $I(q)$ vs q.

morphologies are observed. No aggregates are observed for low carboxyl ion concentration zinc and cobalt ionomers, but spherical aggregates are observed for high carboxyl ion concentration zinc ionomers. Low mol % gallium ionomers have an inhomogeneous distribution of spherical aggregates that are polydisperse in size whereas barium ionomers show rod and bundles of rod-shaped aggregates. The rod-shaped aggregate in ionomer morphology has been observed for the first time. We postulate that the final equilibrium mechanical property of the network is controlled more by the ionic triplets or quartets rather than by the aggregates.

Acknowledgment. This work was supported by the National Science Foundation Polymers Program under Grant DMR-0349952. This work made use of the Cornell Center for Materials Research supported through the National Science Foundation Materials Research Science and Engineering Centers program (Award DMR-0079992) and equipment provided by Department of Energy Grant: DE-FG02-97ER62443. K.I.W. acknowledges the support of NSF-DMR02-35106 and DAAD19-03-1-0130 (U.S. Army). T. M. Duncan, F. Escobedo, and D. Bhawe are also acknowledged for useful discussions.

References and Notes

(1) Register, R. A.; Prud'homme, R. K. In *Ionomers: Synthesis, Structure, Properties and Applications*; Tant, M. R., Mauritz, K. A., Wilkes, G. L., Eds.; Chapman & Hall: New York, 1997; pp 208−260.
(2) Eisenberg, A.; Kim, J. S. *Introduction to Ionomers*; Wiley: New York, 1998; pp 86−189.
(3) Jérôme, R.; Mazurek, M. In *Ionomers: Synthesis, Structure, Properties and Applications*; Tant, M. R., Mauritz, K. A., Wilkes, G. L., Eds.; Chapman & Hall: New York, 1997; pp 16−18.
(4) Jérôme, R.; Mazurek, M. In *Ionomers: Synthesis, Structure, Properties and Applications*; Tant, M. R., Mauritz, K. A., Wilkes, G. L., Eds.; Chapman & Hall: New York, 1997; pp 16−18.
(5) Williams, C. E.; Russell, T. P.; Jérôme, R.; Horrion, J. *Macromolecules* **1986**, *19*, 2877−2884.
(6) Jérôme, R. *Telechelic Polymers: Synthesis and Applications*; Goethals, E. J., Ed.; CRC: Boca Raton, FL, 1989; Chapter 11.
(7) Vanhoorne, P.; Jérôme, R. In *Ionomers: Characterizations, Theory and Applications*; Schlick, S., Ed.; CRC: Boca Raton, FL, 1996; Chapter 9.
(8) Register, R. A.; Foucart, M.; Jérôme, R.; Ding, Y. S.; Cooper, S. L. *Macromolecules* **1988**, *21*, 1009−1015.
(9) Lee, D. C.; Register, R. A.; Yang, C. Z.; Cooper, S. L. *Macromolecules* **1988**, *21*, 998−1004.
(10) Lee, D. C.; Register, R. A.; Yang, C. Z.; Cooper, S. L. *Macromolecules* **1988**, *21*, 1005−1008.
(11) Ding, Y. S.; Register, R. A.; Yang, C. Z.; Cooper, S. L. *Polymer* **1989**, *30*, 1204−1212.
(12) Ding, Y. S.; Register, R. A.; Yang, C. Z.; Cooper, S. L. *Polymer* **1989**, *30*, 1213−1220.
(13) Visser, S. A.; Cooper, S. L. *Macromolecules* **1991**, *24*, 2576−2583.
(14) Visser, S. A.; Cooper, S. L. *Polymer* **1992**, *33*, 920−929.
(15) MacKnight, W. J.; Taggart, W. P.; Stein, R. S. *J. Polym. Sci. Symp.* **1974**, *45*, 113−128.
(16) Roche, E. J.; Stein, R. S.; Russell, T. P.; MacKnight, W. J. *J. Polym. Sci., Polym. Phys.* **1980**, *18*, 1497−1512.
(17) Fujimura, M.; Hashimoto, T.; Kawai, H. *Macromolecules* **1981**, *14*, 1309−1315.
(18) Marx, C. L.; Caulfield, D. L.; Cooper, S. L. *Macromolecules* **1973**, *6*, 344−353.
(19) Yarusso, D.; Cooper, S. L. *Macromolecules* **1983**, *16*, 1871−1880.
(20) Yarusso, D.; Cooper, S. L. *Polymer* **1985**, *26*, 371−378.
(21) Ding, Y. S.; Hubbard, S. R.; Hodgson, K. O.; Register, R. A.; Cooper, S. L. *Macromolecules* **1988**, *21*, 1698−1703.
(22) Register, R. A.; Cooper, S. L. *Macromolecules* **1990**, *23*, 310−317.
(23) Register, R. A.; Cooper, S. L. *Macromolecules* **1990**, *23*, 318−323.
(24) Wu, D. Q.; Chu, B.; Lundberg, R. D.; MacKnight, W. J. *Macromolecules* **1993**, *26*, 1000−1007.
(25) Chu, B.; Wu, D. Q.; Lundberg, R. D.; MacKnight, W. J. *Macromolecules* **1993**, *26*, 994−999.
(26) Laurer, J. H.; Winey, K. I. *Macromolecules* **1998**, *31*, 9106.
(27) Winey, K. I.; Laurer, J. H.; Kirkmeyer, B. P. *Macromolecules* **2000**, *33*, 507−513.
(28) Kirkmeyer, B. P.; Weiss, R. A.; Winey, K. I. *J. Polym. Sci., Part B: Polym. Phys.* **2001**, *39*, 477−483.
(29) Kirkmeyer, B. P.; Taubert, A.; Kim, J.-S.; Winey, K. I. *Macromolecules* **2002**, *35*, 2648−2653.
(30) Taubert, A.; Winey, K. I. *Macromolecules* **2002**, *35*, 7419−7426.
(31) Taubert, A.; Wind, J. D.; Paul, D. R.; Koros, W. J.; Winey, K. I. *Polymer* **2003**, *35*, 1881−1892.
(32) Batra, A.; Cohen, C.; Duncan, T. M. *Macromolecules* **2006**, *39*, 426−438.
(33) Tate, M. W.; Eikenberry, E. F.; Barna, S. L.; Wall, M. E.; Lowrance, J. L.; Gruner, S. M. *J. Appl. Crystallogr.* **1995**, *28*, 196−205.
(34) Mitchell, G. R.; Odajima, A. *Polym. J.* **1984**, *16*, 351−357.
(35) Visser, S. A.; Cooper, S. L. *Macromolecules* **1991**, *24*, 2584−2593.

MA052275A